Theoretical study of permselective layers on amperometric electrodes in flowing streams

ARTICLE *in* ANALYTICAL CHEMISTRY · OCTOBER 1991

Impact Factor: 5.64 · DOI: 10.1021/ac00020a013

3 AUTHORS, INCLUDING:

John Cassidy
Dublin Institute of Technology
76 PUBLICATIONS **815** CITATIONS
SEE PROFILE

Michael E G Lyons
Trinity College Dublin
123 PUBLICATIONS **2,274** CITATIONS
SEE PROFILE

Theoretical Study of Permselective Layers on Amperometric Electrodes in Flowing Streams

William Breen and John F. Cassidy*

Department of Chemistry, Dublin Institute of Technology, Kevin Street, Dublin 8, Ireland

Michael E. G. Lyons

Physical Chemistry Laboratory, University of Dublin, Trinity College, Dublin 2, Ireland

A model consisting of the response of a porous permselective coating on an electrode in an amperometric configuration is solved for two types of concentration profile impinging on the polymer solution interface. A Gaussian concentration profile and a Poisson concentration profile are examined, since both profiles typically arise in both flow injection analysis (FIA) and high-performance liquid chromatography (HPLC). Analytical expressions for current and for concentration profiles within the layer are derived. Working curves are presented that allow estimation of peak height decrease, peak broadening, lag time, and diffusional tailing due to coating the amperometric detector with a permselective layer. It is possible by using these equations and working curves to estimate the diffusion coefficient of substrate through the layer and to design layers which minimize lag time and peak tailing and optimize peak height.

INTRODUCTION

Electrochemical detectors in both flow injection analysis (FIA) and in liquid chromatography (LC) are being used increasingly in analytical chemistry (*1–3*). Modification of the electrode using permselective coatings has been shown to allow greater selectivity for various compounds in a wide range of complex matrices (*4–18*). In this laboratory a sensor for ascorbic acid has been developed and is based on a conducting polymer, polypyrrole-containing dodecylbenzenesulfonate, as a counterion (*19*). This polymer-coated electrode was shown to exhibit enhanced stability and was less prone to surface fouling than the bare platinum electrode. When complex matrices such as fruit juices were examined, surface fouling caused a loss of signal. To overcome this problem a filtering layer such as polyacrylamide was employed in a bilayer configuration with the conducting polymer. A similar approach has been utilized by other workers for the in vivo analysis of dopamine where a Nafion-coated microelectrode was employed (*20*).

It is to be expected that permselective coatings will affect the diffusion of analyte to the underlying sensing layer. The diffusional distortion caused by the presence of such a layer has previously been examined theoretically for a simple concentration step at a polymer-coated electrode (*20–22*). The use of concentration steps is not common practice and therefore a situation frequently encountered in FIA and HPLC is considered in this communication. This consists of the dispersion of a plug of analyte in a flowing stream that is detected at an electrode coated with a permselective polymer layer. The two profiles examined are a Gaussian concentration profile and a Poisson concentration profile. The former occurs due to dispersion of a plug in long narrow tubes, and the latter occurs in short tubes (*23, 24*). Therefore the concentration distribution will pass from Poisson to Gaussian as it moves further down the tube. A solution to the problem of a Gaussian concentration profile impinging on an electrode coated with a permselective layer has been found numerically (*22*) by using orthogonal collocation. However, an analytical solution to the problem would be more useful, since it would allow workers in the area to prepare their own working curves without the need for excessive computation. Such an analysis would be of value to those who use membrane-based electrodes, such as the Clark cell, for sensing in flowing streams (*25*). Other areas to which this theory may apply are flow systems that employ thermistor-based detectors (*26*) or enzyme-containing layers (*27, 28*).

* To whom correspondence should be addressed.

THEORY

The analysis presented in this paper is based on the model shown in Figure 1. This model involves an electrode coated with a thin permselective layer of thickness d as an amperometric detector in a flowing stream. It is assumed that the substrate can permeate into the layer but interferences cannot. It is also assumed that the detector does not affect the laminar flow of the liquid in the flowing stream. The electrode is held at a potential where the substrate is completely oxidized, n electrons being transferred. Migration and convection are assumed to be negligible within the layer, and therefore the mass transport of the analyte to the electrode surface is governed by the diffusion equation.

$$\partial C/\partial t = D\,\partial^2 C/\partial x^2 \qquad (1)$$

where C is the concentration, t is the time, x is the distance away from the electrode, and D is the diffusion coefficient of the substrate within the film.

The concentration profile of the analyte at the polymer solution interface is taken to be either Gaussian or Poisson in time. Both profiles have been shown to exist in flowing streams under certain practical conditions (*23, 24*). A plug of analyte in a flowing stream undergoes dispersion due to both convection and diffusion. The early stages of dispersion are primarily due to convection, which leads to a parabolic concentration profile. The next stage of dispersion involves both convection and diffusion. Both of these stages can be approximated by a Poisson type concentration profile. The final stage is controlled primarily by diffusion leading to a Gaussian type concentration profile (*23*). For these reasons the Gaussian profile can be used to describe the dispersion of a plug of analyte in long narrow tubes whereas the Poisson is more applicable to the treatment of the dispersion in short tubes. A parametric statement can be formulated indicating when the use of a Gaussian concentration profile is appropriate (*23*). This statement relates the tube radius, R, the mean fluid velocity, $\nu°$, and the diffusion coefficient of the analyte, D. A Gaussian concentration profile will be appropriate if $R\nu°/D \gg 7$. This statement can also be given in terms of the resi-

0003-2700/91/0363-2263$02.50/0

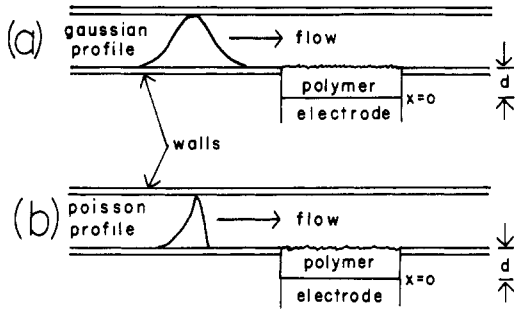

Figure 1. Schematic representation of an electrode modified with a permselective polymer in a flowing stream. Two concentration profiles are represented: (a) a Gaussian concentration profile and (b) a Poisson concentration profile. The polymer layer thickness is d. In practice the electrode need not be sunk in the tube or cell walls, and a thin polymer coating which does not interfere with the laminar flow would also obey this model.

dence time of the substrate in the tube, T, where the Gaussian concentration profile will arise if $T \gg R^2/3.8^2D$. If the above conditions are satisfied and the zone of substrate introduced into the flowing stream is narrower than the tube radius, then the concentration profile will be Gaussian in nature (*23*). The Poisson concentration profile can be shown to be applicable at all stages of dispersion (*23*).

Gaussian Concentration Profile. The method employed to solve the nonhomogeneous boundary value problems was the Sturm–Liouville (*29*) method. The diffusion equation, eq 1, was solved subject to two boundary conditions and an initial condition. The boundary condition at the electrode surface is

$$C(0,t) = 0 \qquad t \geq 0 \tag{2}$$

since the electrode potential is such that the reaction is under diffusion control. Before injection the concentration of the analyte at the electrode surface is zero. Thus the initial condition is

$$C(x,0) = 0 \qquad 0 < x < d \tag{3}$$

prior to injection of the sample. As an approximation to a Gaussian concentration profile at the polymer solution interface, the following equation was used:

$$C(d,t) = \kappa C^* \exp\left[-\frac{1}{2}\left(\frac{t-\mu}{\sigma}\right)^2\right] \tag{4}$$

where C^* is the peak concentration of species injected into the FIA system and κ is the partition coefficient for the substrate within the layer. The mean time and the standard deviation about this mean time are represented by μ and σ, respectively. The mathematics are simplified greatly if the following dimensionless parameters are used:

$$\xi = x/d \qquad \zeta = C/\kappa C^* \qquad \tau = Dt/d^2$$
$$\varphi = D\mu/d^2 \qquad \eta = D\sigma/d^2 \tag{5}$$

The diffusion equation now takes the following form:

$$\partial\zeta/\partial\tau = \partial^2\zeta/\phi\xi^2 \tag{6}$$

subject to

$$\zeta(0,\tau) = 0 \qquad \text{and} \qquad \zeta(\xi,0) = 0 \tag{7}$$

$$\zeta(1,\tau) = \exp(-y^2/2) \tag{8}$$

where y is defined as

$$y = \left(\frac{\tau-\varphi}{\eta}\right) \tag{9}$$

A function is now defined that will allow a transformation of the nonhomogenous boundary condition, eq 8, to a homogenous boundary condition and a nonhomogenous differential equation. This is achieved by defining a function $\upsilon(\xi,\tau)$ as follows:

$$\upsilon(\xi,\tau) = \xi \exp(-y^2/2) \tag{10}$$

and assuming that $\zeta(\xi,\tau) = u(\xi,\tau) + \upsilon(\xi,\tau)$. Where $u(\xi,\tau)$ and $\upsilon(\xi,\tau)$ are independent functions. It can be shown that the boundary value problem, eq 6–8, reduces to

$$\frac{\partial u}{\partial\tau} = \frac{\partial^2 u}{\partial\xi^2} + \frac{y}{\eta}\xi \exp(-y^2/2) \tag{11}$$

where $u(\xi,\tau)$ is subject to the following conditions:

$$u(0,\tau) = 0 \qquad \text{and} \qquad u(1,\tau) = 0 \tag{12}$$

$$u(\xi,0) = -\xi \exp[-1/2(\varphi/\eta)^2] \tag{13}$$

It is then necessary to evaluate the eigenvalues and the eigenfunctions for the corresponding homogenous problem, which is the basic diffusion equation outlined in eq 6 subject to the boundary conditions in eq 12. This problem is solved by separation of variables (*29*). The resulting eigenvalues are

$$\lambda_p = -p^2\pi^2 \qquad p = 1, 2, 3, \ldots \tag{14}$$

The corresponding normalized eigenfunctions are

$$\Phi_p(\xi) = 2^{1/2} \sin(p\pi\xi) \qquad p = 1, 2, \ldots \tag{15}$$

The Sturm–Liouville approach is based on the assumption that the solution $u(\xi,\tau)$, the initial condition, and the nonhomogeneity, $(y/\eta)\xi \exp(-y^2/2)$, can be expanded in terms of the eigenfunctions $\Phi_p(\xi)$. Back-substitution then leads to an ordinary differential equation in τ. Thus it is assumed that

$$u(\xi,\tau) = 2^{1/2}\sum_{p=1}^{\infty} T_p(\tau) \sin(p\pi\xi) \tag{16}$$

Thus expansion of the inhomogeneity in the differential equation, eq 11, leads to

$$\frac{y}{\eta}\xi \exp(-y^2/2) = 2^{1/2}\sum_{p=1}^{\infty} F_p(\tau) \sin(p\pi\xi) \tag{17}$$

Both $T_p(\tau)$ and $F_p(\tau)$ are functions dependent only on time and represent the time-dependent portion of the series approximations. The coefficient $F_p(\tau)$ may be evaluated as follows:

$$F_p(\tau) = \frac{2^{1/2}}{\eta} y \exp(-y^2/2) \int_0^1 \xi \sin(p\pi\xi)\, d\xi \tag{18}$$

leading to the expression

$$F_p(\tau) = \frac{2^{1/2}}{\eta} \frac{(-1)^{p+1}}{p\pi} y \exp(-y^2/2) \tag{19}$$

The initial condition is treated in a similar manner

$$\alpha_p = -2^{1/2} \exp[-1/2(\varphi/\eta)^2] \int_0^1 \xi \sin(p\pi\xi)\, d\xi \tag{20}$$

leading to

$$\alpha_p = 2^{1/2}\frac{(-1)^p}{p\pi} \exp[-1/2(\varphi/\eta)^2] \tag{21}$$

Resubstitution of eq 16 and 19 into eq 11 leads to

$$\sum_{p=1}^{\infty} [T'_p(\tau) + p^2\pi^2 T_p(\tau) - F_p(\tau)] \sin(p\pi\xi) = 0 \tag{22}$$

where $T'_p(\tau)$ represents the first-order partial derivative of $T_p(\tau)$. For this to be true for all ξ, $0 < \xi < 1$ then

$$T'_p(\tau) + p^2\pi^2 T_p(\tau) - F_p(\tau) = 0 \tag{23}$$

This simple first-order differential equation can be solved by employing an integrating factor. Taking the initial condition into account leads to the following solution for $T_p(\tau)$:

$$T_p(\tau) = \alpha_p e^{-p^2\pi^2\tau} + e^{-p^2\pi^2\tau}\int_0^\tau e^{p^2\pi^2 s}F_p(s)\,ds \quad (24)$$

where s is a dummy variable for τ. It is found that the integral present in eq 24 does not have a solution in closed form and so its solution requires a numerical method. Substituting this equation into eq 16 and employing the original assumption that $\zeta(\xi,\tau) = u(\xi,\tau) + v(\xi,\tau)$ yields an explicit expression for $\zeta(\xi,\tau)$

$$C(x,t) = 2\kappa C^*\sum_{p=1}^{\infty}\frac{(-1)^p}{p\pi}e^{-p^2\pi^2\tau}\left[e^q - \int_0^\tau e^{p^2\pi^2 s}(y/\eta)e^j\,ds\right]\sin(p\pi\xi) + \xi\exp(j) \quad (25)$$

where $q = -1/2(\varphi/\eta)^2$, $j = -1/2y^2$, κ is the partition coefficient of the analyte for a given solvent and polymer film, and C^* is the peak concentration of the analyte in the stream. At this point the boundary conditions can be simply checked to show that the solution is valid. The current density has an expression of the following form:

$$i = nFAD\left.\frac{\partial C}{\partial x}\right|_{x=0} \quad (26)$$

where n is the number of electrons transferred in the reaction. Converting dimensioned parameters in eq 26 to dimensionless parameters results in the following:

$$i = \frac{nFAD\kappa C^*}{d}\left.\frac{\partial\zeta}{\partial\xi}\right|_{\xi=0} \quad (27)$$

Thus the following explicit expression for current density is obtained:

$$i = \frac{nFAD\kappa C^*}{d}\left\{2\sum_{p=1}^{\infty}(-1)^p e^{-p^2\pi^2\tau}\left[e^q - \int_0^\tau e^{p^2\pi^2 s}(y/\eta)e^j\,ds\right] + e^j\right\} \quad (28)$$

Poisson Concentration Profile. The assumption on which the derivation of the Poisson equation is based is that the tube through which the analyte is flowing is divided into q small imaginary reactors or tanks in series. The concentration–time distribution predicted by such a model is Poisson in nature. This model is analogous to the theoretical plate model encountered in chromatography or distillation (*23*). In such cases, if the reactors are considered separately, the resulting distribution is binomial in nature. If continuous flow is considered, a Poisson distribution is obtained (*23*). The residence time of the analyte in the tube T_r can then be divided by the number of tanks to give the residence time for the analyte in one tank, T_i. The dimensionless residence time can be defined as $\vartheta = DT_i/d^2$. Therefore the dimensionless differential equation is of the same form as that given in eq 6 and 7 with the boundary condition at the polymer solution interface taking the following form:

$$\zeta(1,\tau) = (\tau/\vartheta)^q e^{-\tau/\vartheta}/q! \quad (29)$$

We now perform a transformation that will convert the boundary condition in eq 29 to a time-independent boundary condition. This is again achieved by defining a function $v(\xi,\tau)$ and assuming that $\zeta(\xi,\tau) = u(\xi,\tau) + v(\xi,\tau)$. Here we define

$$v(\xi,\tau) = \xi(\tau/\vartheta)^q e^{-\tau/\vartheta}/q! \quad (30)$$

With this function and the above transformation the problem now becomes

$$\frac{\partial u}{\partial\tau} = \frac{\partial^2 u}{\partial\xi^2} - \frac{\xi q\tau^{q-1}}{\vartheta^q}\frac{e^{-\tau/\vartheta}}{q!} + \left(\frac{\tau}{\vartheta}\right)^q\frac{\xi}{q!\vartheta}e^{-\tau/\vartheta} \quad (31)$$

subject to

$$u(0,\tau) = 0 \qquad u(1,\tau) = 0 \qquad u(\xi,0) = 0 \quad (32)$$

The eigenvalues and normalized eigenfunctions of the corresponding homogenous problem are the same as those in the previous problem eqs 14 and 15. Again it is assumed that

$$u(\xi,\tau) = 2^{1/2}\sum_{p=1}^{\infty}T_p(\tau)\sin(p\pi\xi) \quad (33)$$

The expansion of the inhomogeneity follows the same approach as that employed in eqs 17–19. Thus

$$F_p(\tau) = -\frac{q\tau^{q-1}}{\vartheta^q}\frac{e^{-\tau/\vartheta}}{q!}2^{1/2}\int_0^1\xi\sin(p\pi\xi)\,d\xi + \left(\frac{\tau}{\vartheta}\right)^q\frac{e^{-\tau/\vartheta}}{q!\vartheta}2^{1/2}\int_0^1\xi\sin(p\pi\xi)\,d\xi \quad (34)$$

leading to

$$F_p(\tau) = \frac{(-1)^{p+1}}{p\pi}\left[\frac{-2^{1/2}\tau^{q-1}e^{-\tau/\vartheta}}{(q-1)!\vartheta^q} + \frac{2^{1/2}e^{-\tau/\vartheta}}{q!\vartheta}\left(\frac{\tau}{\vartheta}\right)^q\right] \quad (35)$$

The initial condition being zero leads to the following:

$$\alpha_p = 0 \quad (36)$$

Thus these expressions can be substituted into eq 24 leading to the following expression for $T_p(\tau)$:

$$T_p(\tau) = \frac{2^{1/2}(-1)^p}{pq!\vartheta^q\pi}e^{-p^2\pi^2\tau}\left(\int_0^\tau e^{zs}qs^{q-1}\,ds - \int_0^\tau\frac{e^{zs}s^q}{\vartheta}\,ds\right) \quad (37)$$

$$z = p^2\pi^2 - \frac{1}{\vartheta} \quad (38)$$

Substitution of this expression into eq 33 yields an expression for $u(\xi,\tau)$. Utilizing the relationship $\zeta(\xi,\tau) = u(\xi,\tau) + v(\xi,\tau)$ results in an expression for the concentration profile in time and distance. Thus

$$\zeta(\xi,\tau) = \sum_{p=1}^{\infty}\frac{2(-1)^p}{\vartheta^q\pi q!p}e^{-p^2\pi^2\tau}\left(\int_0^\tau e^{zs}qs^{q-1}\,ds - \int_0^\tau\frac{e^{zs}s^q}{\vartheta}\,ds\right)\sin(p\pi\xi) + \xi\left(\frac{\tau}{\vartheta}\right)^q\frac{e^{-\tau/\vartheta}}{q!} \quad (39)$$

With eq 26 the current density can be found.

$$j = \frac{nFADC^*\kappa}{q!d\vartheta^q}\left[\sum_{p=1}^{\infty}2(-1)^p e^{-p^2\pi^2\tau}\left(\int_0^\tau e^{zs}qs^{q-1}\,ds - \int_0^\tau\frac{e^{zs}s^q}{\vartheta}\,ds\right) + (\tau)^q e^{-\tau/\vartheta}\right] \quad (40)$$

The two integrals in eq 40 can be evaluated simply by using reduction formulas that are amenable for use on a computer. Thus if we set

$$I_{r,A} = \int_0^\tau e^{(p^2\pi^2 - 1/\vartheta)s}qs^{r-1}\,ds \quad (41)$$

where r is a dummy variable replacement for q for the determination of the reduction formulas, a reduction formula of the form

$$I_{r,A} = q\left[\frac{s^{r-1}}{p^2\pi^2 - 1/\vartheta}e^{(p^2\pi^2 - 1/\vartheta)s} - \frac{(r-1)}{p^2\pi^2 - 1/\vartheta}I_{r-1,A}\right]_0^\tau \quad (42)$$

is obtained. If the expression

$$I_{r,B} = \frac{1}{\vartheta}\int_0^\tau e^{(p^2\pi^2-1/\vartheta)s}s^r\,ds \tag{43}$$

is employed, then the reduction formula obtained for this integral is

$$I_{r,B} = \frac{1}{\vartheta}\left[\frac{s^r}{p^2\pi^2 - 1/\vartheta}e^{(p^2\pi^2-1/\vartheta)s} - \frac{r}{p^2\pi^2 - 1/\vartheta}I_{r-1}\Big|_0^\tau\right] \tag{44}$$

For the complete evaluation of the reduction formulas, the solution of the integrals when $r = 1$ and $r = 0$ for eqs 42 and 44, respectively, are required and are as follows:

$$I_{1,A}/q = \vartheta I_{0,B} = \frac{e^{(p^2\pi^2-1/\vartheta)\tau}}{p^2\pi^2 - 1/\vartheta} - \frac{1}{p^2\pi^2 - 1/\vartheta} \tag{45}$$

RESULTS AND DISCUSSION

Gaussian Concentration Profile. As $\sigma \to \infty$ the Gaussian concentration profile should approach that of a concentration step. This problem has been solved by Engstrom et al. (*21*) and this group (*22*). Thus the current density due to the concentration step should be equal to that of a Gaussian concentration profile with an infinite standard deviation. As the dimensionless standard deviation η in eq 28 approaches infinity, both j and $q \to 0$ and the expression reduces to

$$i = \frac{nFADKC^*}{d}[1 + 2\sum_{p=1}^{\infty}(-1)^p e^{-p^2\pi^2\tau}] \tag{46}$$

Remembering that the time τ is dimensionless and replacing it with

$$\tau = Dt/d^2 \tag{47}$$

we obtain the same expression for the current density as that previously presented by Engstrom (*21*) and by this laboratory (*22*). The numerical solution of the above problem where the incident Gaussian concentration profile has an infinite standard deviation produces an identical result (*22*).

The generation of working curves from eq 28 was performed with a basic program run on an "IBM compatible" Amstrad 1512 computer. The integral was solved using Simpson's rule utilizing 50 subintervals.

A dimensionless plot of the concentration gradient at the electrode surface against time, for an input profile with the peak in the concentration occurring at a dimensionless time of 0.3 and with a dimensionless deviation of 0.1 is presented in Figure 2. The resulting signal exhibits a peak at a dimensionless time of 0.44. Thus the dimensionless lag time, which is the difference in the dimensionless time at which the peak in concentration occurs at the polymer solution interface and the dimensionless time of the signal peak, is 0.14 and is independent of thickness. This is in reasonable agreement with the dimensionless lag time of 0.1349 found by employing numerical techniques (*22*). The value of 0.14 was obtained from a computer program that calculated the current at intervals of 0.01 in the dimensionless time from 0 to 1. When the interval size is decreased to 8×10^{-4}, a dimensionless lag time of 0.1384 is obtained by using four terms in the summation. The number of terms in the summation in eq 28 was varied, and for the conditions employed in Figure 2, four terms in the summation were found to yield a peak current that differed in magnitude from that obtained by using numerical techniques by less than 4%. Increasing the number of terms to 6 yielded a value that differed from that obtained numerically by ca. 2%, and increasing the number of terms to 10 produced little change in this discrepancy. The presence of the $\exp(p^2\pi^2 s)$ term inside the integral in eq 28 limits the number of terms that can be employed, since such a function can produce very large numbers depending on the value of s and the number of terms employed p. For example for p = 8 and s = 0.6, this expression yields a value of ca. 3.844×10^{164}. The use of double precision in computer programming permits numbers as large as 10^{308}. As a result of this it has been found that under the conditions employed for Figure 2 the maximum number of terms is ca. 10. It is possible to employ a greater number of terms at short dimensionless times but at longer times, closer to $\tau = 1$, overloading occurs on the PC. However the error involved in using eq 28 is as low as 2% over the data obtained by using orthogonal collocation techniques for this system (*22*). The number of terms required in the summation was found to depend also on the magnitudes of D and d.

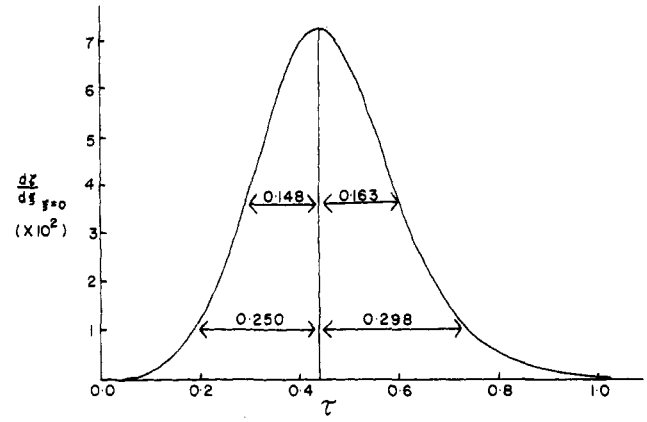

Figure 2. Dimensionless plot of concentration gradient at the electrode surface against time for a Gaussian concentration profile at a polymer-coated electrode in a flowing stream. The number of terms employed in the summation was 4 with 50 subintervals for the Simpson's rule subroutine for the evaluation of the integral. The input Gaussian peak had a mean time of 0.3 and a standard deviation of 0.1. Diffusional tailing can clearly be seen. The dimensionless mean and deviation can be related to dimensioned values by employing eq 5.

The resulting signal peak is also asymmetrical as a result of diffusional tailing. Diffusional tailing occurs as a result of the concentration gradient at the polymer solution interface changing sign after the concentration peak in solution has passed. This leads to an equilibrium situation that prolongs the time taken for the electrode to sense the maximum in solution concentration.

Figure 3 exhibits the effect of layer thickness on the general shape of the resulting signal in real time. Peak broadening and a reduction in the peak height along with a greater lag time are more evident on increasing the layer thickness, as is the extent of diffusional tailing. It can be seen that a thinner layer exhibits a greater signal; however this is at the expense of selectivity.

The incorporation of a flow rate dependence for the above set of equations can be achieved by replacement of the deviation σ by an equation describing dispersion (*23*)

$$\sigma = [(R\nu^\circ)^2 t/24D^*]^{1/2} \tag{48}$$

where R is the tube radius, ν° is the mean fluid velocity, D^* is the diffusion coefficient for the analyte in solution, and t is the time. In this case it can be seen that σ has units of distance and that the terms t and μ in eq 28 must be transposed into distance terms such as $z = \nu^\circ t$ and $\nu^\circ\mu$. The linear velocity term ν° can then be related to the volume flow rate F_m by using $\nu^\circ A^* = F_m$ where A^* is the cross sectional area of the tube.

Poisson Concentration Profile. With eqs 40, 42, 44, and 45 working curves can be generated. A plot of the dimensionless concentration gradient at the electrode surface against dimensionless time is presented in Figure 4. The plot exhibits a broadness more associated with a Gaussian profile than with a Poisson profile. This would appear to be due to the coupling

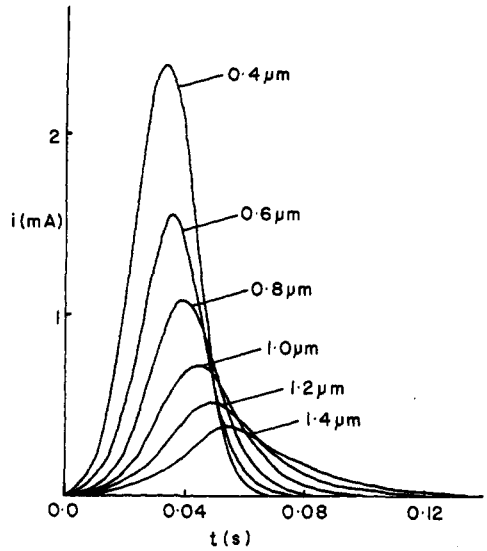

Figure 3. Study of the effect of varying layer thickness on the shape of the resulting current signal. The number of terms in the summation was 4 in each case with 50 subintervals for the Simpson's rule subroutine. The electrode area was taken to be 1 cm^2, the diffusion coefficient of the analyte within the layer, $D = 1 \times 10^{-7}$ cm^2 s^{-1}, $C^* = 1 \times 10^{-5}$ mol dm^{-3}, and $\kappa = 1$. The input Gaussian profile had a mean of $\mu = 0.03$ s and a standard deviation of $\sigma = 0.01$ s.

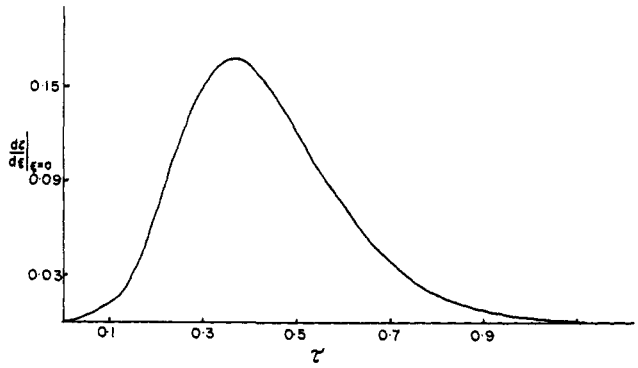

Figure 4. Dimensionless plot of the concentration gradient at the electrode surface against time. The dimensionless residence time for the analyte in the tube was taken to be 0.2, and the number of terms employed in the summation was 4. The number of tanks was taken as 3. The dimensionless lag time calculated from the peak signal time was 0.156.

of the Poisson concentration profile and the diffusion process through the layer. The lag time is found to be 0.156. This is somewhat larger than that found for the Gaussian concentration profile and may be a result of the rapid decrease in concentration at the polymer solution interface after the peak in the Poisson distribution. This would have the effect of enhancing the diffusional tailing and slowing the diffusion toward the electrode surface, thereby increasing the lag time. The number of terms required in the summation, above which no change in the magnitude of the data occurs, was found to depend on the magnitude of the retention time chosen and to a smaller extent on the number of theoretical plates. Usually four terms in the summation were employed. Increasing this to ten terms produced no change in the lag time and a change of 1.8% in the magnitude of the peak current. The problem associated with the $\exp(p^2\pi^2\tau)$ term is also present in this case and limits the number of terms that can be employed for the deduction of the signal profile. Once again the dimensionless plot applies for all possible chosen values of D and d.

Figure 5 exhibits the dependence of the peak shape on the number of tanks in series as outlined above. It is found that the peak height decreases as well as the area under the peak. Mathematically, as the number of tanks increases toward

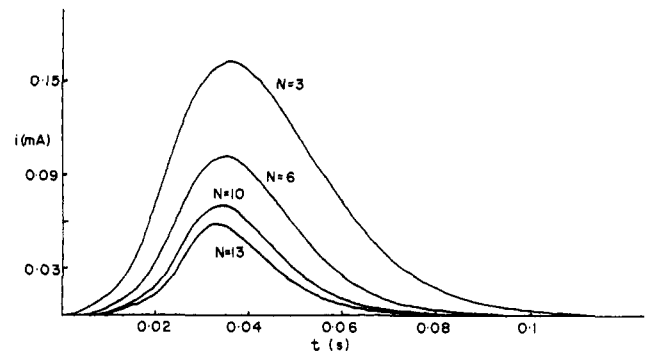

Figure 5. Dependence of the general peak shape on the number of tanks in series. The input parameters were $D = 1 \times 10^{-7}$ cm^2 s^{-1}, $C^* = 1 \times 10^{-5}$ mol dm^{-3}, and $d = 1 \times 10^{-4}$ cm. The number of terms employed in the summation was 4, and the retention time was input as 0.2 s.

infinity, the tube length increases and the Poisson profile should tend toward a Gaussian profile. In reality this would occur as a result of a combination of convection and diffusion causing an asymmetric broadening of the concentration profile. This results in a loss of signal due to the smaller concentration gradient at the solution polymer interface. It is also found that as the layer thickness is increased, the lag time increases in a manner similar to that in the Gaussian case discussed previously.

CONCLUSION

The results of this work indicate that the deposition of a porous layer on an electrode would result in a signal peak broadening, a decrease in peak height and an increase in lag time. By using eqs 28 and 40 optimization of the layer thickness is possible, providing the diffusion coefficient of the analyte within the layer can be estimated. With a knowledge of the concentration profile, working curves can be generated that would allow optimization of the response obtained at the detector. A useful application of these working curves is in the choice of a layer thickness that would result in a response ca. 90% of that obtained for the uncoated electrode. In this situation a reasonable sensitivity exhibited by the sensing electrode in the flowing stream would be maintained. The presence of a lag time may also introduce problems with sensitivity in that for thick layers the reduction in peak height is quite large. Thus, use of the dimensionless plots presented in this paper are of value for the determination of layer thickness that would minimize the effects of lag time and yet allow a reasonable thickness for the filtering membrane. The use of the working curves may involve curve fitting of experimental data to the equations for current density presented. However this method may not be suitable because of the large number of parameters in the equations. A more realistic application may involve the use of theoretical peak current versus layer thickness plots or lag time versus layer thickness plots for the optimization of sample throughput and sensitivity.

LIST OF SYMBOLS

A	electrode area
A^*	cross sectional area of the tube
C, $C(x,t)$	concentration of analyte in the film
C^*	peak concentration of analyte in the stream
d	layer thickness
D	diffusion coefficient of the analyte within the film
D^*	diffusion coefficient of the analyte in the stream
F	Faraday's constant
F_m	volume flow rate
$F_p(\tau)$	intermediate function used in the calculation
i	current
I	symbol for the reduction formulas

j	current density
n	number of electrons transferred
p	number of terms over which the summation is evaluated
q	number of tanks into which the tube is divided
R	tube radius
t	time
$T_p(\tau)$	intermediate function used in the calculation
T_i	tank i
$u(\xi,\tau)$	dimensionless component of the concentration
$v(\xi,\tau)$	dimensionless component of the concentration
x	distance perpendicular to the electrode surface
y	dimensionless normalized time
z	intermediate function used in the calculation
α_p	intermediate function used in the calculation
ζ	dimensionless concentration
η	dimensionless standard deviation for the Gaussian profile
κ	partition coefficient of the analyte into the film
λ_p	eigenvalue
μ	mean time for the peak of the concentration profile reaching $x = d$
ξ	dimensionless distance
σ	standard deviation about the mean for the Gaussian concentration profile (This also represents the dispersion of the Poisson concentration profile.)
τ	dimensionless time
ϑ	dimensionless residence time
v°	mean fluid velocity
$\Phi_p(\xi)$	eigenfunction
φ	dimensionless mean for the Gaussian profile

ACKNOWLEDGMENT

We thank the reviewers for their valuable comments.

LITERATURE CITED

(1) Rucki, R. J. *Talanta* **1980**, *27*, 147.
(2) White, P. C. *Analyst* **1984**, *109*, 677.
(3) Štulík, K.; Pacáková, V. *J. Electroanal. Chem. Interfacial Electrochem.* **1981**, *129*, 1.
(4) Sittampalam, G.; Wilson, G. S. *Anal. Chem.* **1983**, *55*, 1608.
(5) Wang, J.; Hutchins, L. D. *Anal. Chem.* **1985**, *57*, 1536.
(6) Hutchins-Kumar, L.; Wang, J.; Tuzhi, P. *Anal. Chem.* **1986**, *58*, 1019.
(7) Wang, J.; Chen, S. P.; Lin, M. S. *J. Electroanal. Chem. Interfacial Electrochem.* **1989**, *273*, 231.
(8) Wang, J.; Tuzhi, P.; Golden, T. *Anal. Chim. Acta* **1984**, *194*, 129.
(9) Ji, H.; Wang, E. *J. Chromatog.* **1987**, *410*, 111.
(10) Wang, J.; Golden, T. *Anal. Chem.* **1989**, *61*, 1597.
(11) Wang, J.; Golden, T.; Tuzhi, P. *Anal. Chem.* **1987**, *59*, 740.
(12) Wang, J.; Tuzhi, P. *Anal. Chem.* **1986**, *58*, 3257.
(13) Wang, J.; Tuzhi, P. *J. Electrochem. Soc.* **1987**, *134*, 586.
(14) Wang, J.; Golden, T.; Li, R. *Anal. Chem.* **1988**, *60*, 1642.
(15) Wang, J.; Li, R. *Talanta* **1989**, *36*, 279.
(16) Wang, J. *Anal. Chim. Acta* **1990**, *234*, 41.
(17) Cassidy, J. F.; O'Donoghue, E.; Breen, W. *Analyst* **1989**, *114*, 1509.
(18) Cassidy, J. F.; Lowney, C. *Anal. Chim. Acta* **1990**, *234*, 479.
(19) Lyons, M. E. G.; Breen, W.; Cassidy, J. F. *J. Chem. Soc., Faraday Trans.* **1991**, *87*, 115.
(20) Kristensen, E. W.; Kuhr, W. G.; Wightman, R. M. *Anal. Chem.* **1987**, *59*, 1752.
(21) Engstrom, R. C.; Wightman, R. M.; Kristensen, E. W. *Anal. Chem.* **1988**, *60*, 652.
(22) Cassidy, J. F.; Breen, W.; Lyons, M. E. G. *Electroanalysis* **1991**, *3*, 293.
(23) Štulík, K.; Pacáková, V. *Electroanalytical Measurements in Flowing Liquids*; Ellis Harwood; Chichester, U.K., 1987.
(24) Betteridge, D. *Anal. Chem.* **1978**, *50*, 832A.
(25) Clark, L. C., Jr. *Trans—Am. Soc. Artif. Intern. Organs* **1956**, *2*, 41.
(26) Mosbach, K.; Danielsson, B. *Anal. Chem.* **1981**, *53*, 83A.
(27) Bradley, C. R.; Rechnitz, G. A. *Anal. Chem.* **1985**, *57*, 1401.
(28) Harrison, J. D.; Turner, R. F. B.; Baltes, H. P. *Anal. Chem.* **1988**, *60*, 2002.
(29) Boyce, W. E.; DiPrima, R. C. *Elementary Differential Equations and Boundary Value Problems*; Wiley: New York, 1986.

RECEIVED for review November 27, 1990. Accepted July 16, 1991. J.F.C. wishes to acknowledge a grant (No. ARP/61) from EOLAS. M.E.G.L. would also like to acknowledge a grant from EOLAS under the strategic research programme.

Amperometric Glucose Microelectrodes Prepared through Immobilization of Glucose Oxidase in Redox Hydrogels

Michael V. Pishko, Adrian C. Michael,[1] and Adam Heller*

Chemical Engineering Department, University of Texas at Austin, Austin, Texas 78712

Glucose microelectrodes have been formed with glucose oxidase immobilized in poly[(vinylpyridine)Os(bipyridine)$_2$Cl] derivative-based redox hydrogels on beveled carbon-fiber microdisk (7 μm diameter) electrodes. In the resulting microelectrode, the steady-state glucose electrooxidation current density is 0.3 mA cm^{-2} and the sensitivity is 20 mA cm^{-2} M^{-1}. The current density and sensitivity are 10 times higher than in macroelectrodes made with the same hydrogel. Furthermore, the current is less affected by a change in the partial pressure of oxygen. The higher current density and lower oxygen sensitivity point to the efficient collection of electrons through their diffusion in the redox hydrogel to the electrode surface. These results contrast with those observed for enzyme electrodes based on diffusing mediators, where loss of the enzyme-reduced mediator by radial diffusion to the solution decreases the current densities of microelectrodes relative to similar macroelectrodes.

* To whom correspondence should be addressed.
[1] Current address: Department of Chemistry, University of Pittsburgh, Pittsburgh, PA 15260.

INTRODUCTION

Among the enzyme-based electrochemical biosensors (*1–4*) for the determination of clinical and industrial analytes, the most widely used and studied are those for glucose. Because glucose oxidase transfers electrons to diffusing and nondiffusing mediators, withstands chemical immobilization techniques, and has a high turnover rate ($\sim 10^3$ s^{-1}) at ambient temperature, this enzyme is commonly used in glucose sensors. Miniaturization of glucose sensors is relevant both to the measurement of glucose in small volumes and in vivo, and size is important in monitoring the dynamics of local chemical events in specific regions of an organ. Sensor miniaturization has allowed in vivo measurements of neurotransmitter release from dopaminergic neurons in mammalian brain tissue with microvoltammetric electrodes (*5*). In addition, microsensors with dimensions smaller than their substrate diffusion layer rapidly attain steady-state conditions via radial mass transport, allowing the use of signal-averaging techniques. Glucose microsensors have been made by using glucose oxidase immobilized on microcylinders, microdisks, and microplanar surfaces (*6–17*). These microsensors measure either the change in oxygen partial pressure (*16*), the concentration of evolved

0003-2700/91/0363-2268$02.50/0